Journal of Materials Chemistry A

Reducing Traps Density and Carriers Concentration by Ge Additive for An Efficient Quasi 2D/3D Perovskite Solar Cell

Journal:	*Journal of Materials Chemistry A*
Manuscript ID	TA-COM-10-2019-011989.R1
Article Type:	Communication
Date Submitted by the Author:	28-Dec-2019
Complete List of Authors:	Ng, Chi Huey; Kyushu Institute of Technology, Life Science and Systems of Engineering Hamada, Kengo; Kyushu Institute of Technology Kapil, Gaurav; University of Tokyo, Kamarudin, Muhammad Akmal; The University of Electro-Communications, Info-Powered Energy System Research Center Wang, Zhen; Kyushu Kogyo Daigaku - Wakamatsu Campus, Graduate School of Life Science and Systems Engineering Iikubo, Satoshi ; Kyushu Kogyo Daigaku - Wakamatsu Campus, Graduate School of Life Science and Systems Engineering Shen, Qing; Denki Tsushin Daigaku Joho Rikogakubu Joho Rikogaku Kenkyuka, Department of Engineering Science Yoshino, Kenji; University of Miyazaki, Department of Electrical and Electronic Engineering Minemoto, Takashi; Ritsumeikan University, Department of Electrical and Electronic Engineering Hayase, Shuzi ; University of Electro-Communications, Info-Powered Energy System Research Center

SCHOLARONE™
Manuscripts

Reducing Traps Density and Carriers Concentration by Ge Additive for An Efficient Quasi 2D/3D Perovskite Solar Cell

Chi Huey Ng [a*], Kengo Hamada [a], Gaurav Kapil [b,c], Muhammad Akmal Kamarudin [c], Zhen Wang [a], Satoshi Iikubo [a], Qing Shen [d], Kenji Yoshino [e], Takashi Minemoto [f], Shuzi Hayase [c*]

[a]Graduate School of Life Science and Systems Engineering, Kyushu Institute of Technology, 2-4 Hibikino, Wakamatsu-ku, Kitakyushu, 808-0196, Japan.

[b]The University of Tokyo, Research Center for Advanced Science and Technology, 4-6-1 Komaba, Meguro-ku, Tokyo, 153-8904, Japan.

[c]Info-Powered Energy System Research Center (i-PERC), The University of Electro-Communications, 1-5-1 Chofugaoka, Chofu, Tokyo, 182-8585 Japan.

[d]Graduate School of Informatics and Engineering, University of Electro-Communication, 1-5-1 Chofugaoka, Chofu, Tokyo, 182-8585, Japan.

[e]Faculty of Engineering, University of Miyazaki, Gakuen-kibanadai-nishi-1-1, Miyazaki, 889-2192, Japan.

[f]Department of Electrical and Electronic Engineering, Ritsumeikan University, 1-1-1 Nojihigashi, Kusatsu, Shiga 525-8577, Japan.

*Corresponding authors e-mail addresses: ngchihuey@yahoo.com; hayase@uec.ac.jp

Abstract

We realize the doping of hydrophobic bulky 2D phenylethylammonium (PEA^+) is desirable to stabilize perovskite matrix and enhance stability. The addition of PEA^+ alters the crystal growth orientation and improves the connectivity of the crystal grains. However, solely adding the PEA^+ material is capable-less to fully passivate the severe bulk recombination sites/interior defects due to Sn vacancies, led to an efficiency of 3.96% (V_{oc} of 0.36 V) for a Ge-free device. Whilst, we find that the addition of a smaller size Ge ions; with an optimum doping concentration, has effectively reduced the leakage current and suppressed the carrier density of the perovskite. From the perspective of traps, the addition of Ge reduces traps, typically deep traps and its effectiveness (Ge) in traps passivation was further deduced from thermally stimulated current (TSC) profile. The total trap density was doubly reduced to $4.14x10^{20}$ cm^{-3} when 7.5 mole% Ge was added, which led to photo-conversion efficiency of 7.45% with a high V_{oc} of 0.46 V. In addition, the defect healing by the Ge additive has significantly enhanced the stability of the un-encapsulated device for 192h. This work shows that Ge is an effective additive to suppress recombination sites (trap states passivation); leading to the establishment of an efficient tin based perovskite solar cell.

Introduction

Attention has recently been steered towards lead-free perovskite solar cells (PSC) by substituting lead to less toxic metals such as tin (Sn) and germanium (Ge).[1,2] Sn has been one of the most potential B-site candidates for the lead-free PSC owing to its high absorption coefficients, small exciton binding energies, and high charge carrier mobilities.[3–5] In addition, Sn perovskites exhibited narrower optical band gap (1.2-1.4 eV), which is closer to the Shockley-Queisser limit (1.34 eV), making them ideally fitted for photovoltaics and optoelectronic devices application. However, one of the challenges for the Sn perovskite is that the easy formation of Sn vacancies owing to its small formation energy and its ease oxidation of Sn^{2+} to Sn^{4+}, which resulted in severe charge carrier recombination losses.[6–11] In addition, the presence of dangling bonds on the Sn perovskite's surface and grain boundaries, and the formation of defects in polycrystalline perovskite films are the causes that induce device's degradation; attributed to the formation of trap states and non-radiative recombination sites.[12–14]

Strategies have been executed to plunge the undesirable background carrier density by adding SnF_2 to suppress its unintentional self p-doping process and to fill the vacancies. In 2014, Kumar et al., reported a 2% efficiency was achieved for a $CsSnI_3$ solar cell upon the addition of 20% SnF_2 as a reducing agent.[15] Subsequently, a doubly increment in efficiency up to 4.8% was reported by Seok and co-workers when SnF_2-pyrazine was incorporated into the $FASnI_3$. They revealed that the addition of SnF_2-pyrazine as the mediator enhanced the film morphology of $FASnI_3$, credited to the slow thin film crystallization rate and the

SnF_2-pyrazine complex mitigated phase separation on the perovskite surface.[16] Additionally, the beneficial effect of SnF_2 on trap suppression was further demonstrated by Ng et al., through thermally stimulated current (TSC). The Sn perovskite without SnF_2 possessed wide TSC signal and huge total trap densities ($5.79x10^{22}$ cm^{-3}), which is one order higher in magnitude than the perovskite with SnF_2 ($1.93x10^{21}$ cm^{-3}). When an optimum amount of Ge was added into the $FA_{0.75}MA_{0.25}Sn_{1-x}Ge_xI_3$ perovskite, it was reported that the Ge ions could filled the defects and Sn vacancies of the perovskite, consequently contributed to significant reduction of trap density to 10^8-10^{14} cm^{-3}.[17,18] Nevertheless, the stability and moisture resistivity of Sn-based PSC could be still restrained by the hydrophilic FA^+ and MA^+ cations, which calls for the development of 2D or quasi-2D perovskite solar cells.

The replacement of the hydrophilic cations with hydrophobic long alkyl chain cations is able to enhance the solar cell's stability.[19–22] G. Kanatzidis and co-workers fabricated quasi-2D Sn_3I_{10} (n = 3) and Sn_4I_{13} (n = 4) PSC, which have exhibited PCE below 3%, but with much improved stability than the 3D $MASnI_3$ PSC.[7,23] With the addition of 20% stoichiometric ratio of phenethylammonium iodide (PEAI) into the $FASnI_3$ perovskite, the PCE was substantially improved to 5.94% and subsequently improved to 9% efficiency when a relatively lower stoichiometric ratio of PEAI was incorporated to FAI, which resulted in excellent stability.[7,24] While Ke et al., reported the best Sn perovskite device at PCE of 7.14% when 10% ethylenediammonium {en} additive was added into the $FASnI_3$ framework. The encapsulated {en}$FASnI_3$ solar cell retained 96% of its initial PCE

after 1000h aging process.[25] Despite the addition of a trace amount of 2D could have passivated the ease oxidizable Sn perovskite from moisture; for stability enhancement. However, they are still suffering from intrinsic and oxidative instability, which could be attributed to the presence of trap states. It is notable that the importance criteria for a solar cell with excellent photo-physical properties and photovoltaic performances is always commensurate to good film quality, which is in regard to low defect states.[17]

In this work, we investigated the effect of Ge on traps landscape and discussed its beneficial impact on charge carrier dynamics of the perovskite material. We combine both the advantages of PEAI and Ge ions as the prime ingredients in Sn perovskite framework for moisture ingression and passivation purposes. Knowing that the hydrophobic PEA^+ cations are capable to improve the perovskite crystallinity and to serve as moisture inhibiting layer, nevertheless, the alteration of the perovskite crystal orientation by bulky 2D chains at certain extent may induce undesirable distortions. More importantly, it is impossible for the bulky 2D chains to be penetrated into the 3D framework for passivation purpose; unless the utilization of a smaller ion such as Ge. Effectively, the introduction of Ge has significantly reduced the energetic depth of the deepest trap states in the system, which contributed to low total trap density of 4.14×10^{20} cm^{-3}, as opposed to the quasi-2D/3D PSC without Ge (9.68×10^{20} cm^{-3}). More importantly, the inclusion of Ge restrained self p-doping, minified undesirable carrier density, and thus contributed to high charge mobility. The addition of an optimum amount of 7.5 mole% Ge has prompted for high PCE of 7.45% with excellent stability.

Results and Discussion

Relative to the pristine FSI cell, the role of PEAI was first explicated with the improved V_{oc} and FF values (Figure 1a and Table 1); contributed to the passivation of surface defect states by the compact hydrophobic PEAI layer. It is speculated that the bulky PEA^+ improves the connectivity of the crystal grains and partially passivates the defects at the grain boundaries, as shown in the scheme 1.[12] Nevertheless, the inclusion of PEA^+ cations could slice the 3D perovskite structure and act as an insulator to retard the internal charge transportation. While, the inclusion of Ge has substantially impacted the photovoltaic performances of the $FA_{0.92}PEA_{0.08}Sn_xGe_{1-x}I_3$ ($FPS_xG_{1-x}I$) solar cells. The Ge-based devices (excluding FPSGI(10.5Ge)) garned higher photocurrent (J_{sc}) response, V_{oc}, and PCE. The best PCE of 7.45% is realized when 7.5 mole% Ge was incorporated; with a high J_{sc} of 21.92 mA/cm^2, high V_{oc} of 0.46, and high FF of 0.73 with negligible hysteresis effect (Figure 1c). The high J_{sc} of the Ge-based solar cells are in great agreement with the absorption spectrum (Figure S1a). The merited photovoltaic performances are also credited to the formation of highly crystalline perovskite materials, as explicated from the XRD profile (Figure S1b). The orthorhombic (*Amm2*) crystal strucure $FASnI_3$ exhibited five dominant diffraction peaks at 14.07°, 24.39°, 28.14°, 31.55°, 40.47° and was indexed to (100), (120)/(102), (200), (122), and (222), respectively, which is consistent with the reports in the literature. The presence of the all five diffraction peaks indicates that FSI is composed of grains with random orientation.[3,6,7] On adding PEAI as an additive, low intensity diffraction peaks (Figure S1c, green pattern) were observed at low diffraction angles, indicates the

presence of 2D perovskite in the 3D FSI matrix. Interestingly, there has no additional peak observed when Ge was added, implies the addition of Ge caused no disruption on the perovskite structure. In addition, the existence of PEAI is further evidenced through SEM (Figure S2) where the FSI film morphology was considerably altered upon the addition of PEAI; with no apparent crystalline grain boundaries (Figure S2b). The addition of PEAI has merged the crystal grains to form continous film, however, the pinholes and grain boundaries were still unambigously observabled. Interestingly, the pinholes were filled when an optimum amount of Ge ions were incorporated (Figure S2c). The role of Ge has further amplified when FPSGI (7.5Ge) has lower dark current density than the Ge-free device (Figure 1d); implies improved charge transport, suppression of charge recombination, and low leakage current, which leads to higher V_{oc} (corroborated with the J-V results).[26–29] The slight increment in dark current density after 0.6 V for the FPSGI (7.5Ge) device is ascribed to lower charge injection barrier, which regards to higher charge recombination resistance.

Thanks to the doubly effects of PEA^+ and Ge^{2+}, the PCE of FPSGI (7.5Ge) was elevated to 7.57% after storage of 192h in the glovebox, as depicted in Figure 1b and S3a. This phenomenon is hypothesized to be due to the effectiveness of PEA^+ in preventing the ingression of moisture and the passivated defect states by the Ge, in addition, the contribution of the iodide source from the Ge ion in stabilizing the SnI_2 proportion. It is expected that the presence of bulky organic molecule (PEAI) could acts as a capped layered to encapsulate the perovskite materials due to its appreciable van der Waals forces that confer stability improvement.[19] The

double positive effect of PEA^+ and Ge^{2+} is further magnified when an un-encapsulated FPSGI (7.5 Ge) solar cell was exposed to continuous illumination at ambient environment where this device retains 70% of its original efficiency after 3h of illumination (Figure S3b). The enhanced stability of the Ge-based device is credited to the passivation effect of Ge and the formation of a thin GeO_2 layer in preventing moisture ingress.[17] The reproducibility of FPSGI with and without Ge is explicated through histogram with Gaussian fitting composed of 25 devices, as displays in Figure 1e and Table S2. Figure 1f shows the IPCE spectrum of $FPS_xG_{1-x}I_3$ perovskite solar cells. A plateau of IPCE (FPSGI(7.5Ge)) around 400-600 nm (~ 70%) implies a high photon-to-electron conversion of the state-of-art and the integrated J_{sc} is in great agreement with the J_{sc} value obtained from the J-V profile.

Whilst, the compromised overall photovoltaic performances of the Ge-free devices such as the J_{sc} and V_{oc} are speculated to be ascribed to the presence of non-desirable trap states (as evidenced through TSC profile). Evidently, both the devices without Ge exhibited low shunt resistances,R_{sh} (12-fold and 2-fold lower for the FSI and FPSGI (0 Ge)), respectively, than the FPSGI (7.5 Ge) (refer to Table S3), probably owing to the occurrence of minor interfacial charge recombination.[26] This phenomenon thus reflected the reason of low J_{sc} and V_{oc} for the Ge-free solar cells. We speculated that the reduced V_{oc} (greater V_{oc} loss) is attributed to the increased trap states across the interfaces and within the perovskite absorber, consequently affects the photovoltaic and stability performances.

The impact of Ge in traps passivation is revealed through TSC, which is a powerful tool to evaluate the trap densities and depths of a semiconducting material. The depth of the trap states in the system was calculted using equation (1).[30,31]

$$E_T = k_B T_m ln(\frac{T_m^4}{\beta}) \quad (1)$$

where k_B is the Boltzmann constant, T_m is the TSC peak's temperature, and β is the heating rate. While the trap density was calculated via equation (2):[30,31]

$$N_t = \frac{Q}{qAL} \quad (2)$$

where Q is the area under TSC graph, q is the electronic charge, A is the active area, and L is the perovskite's thickness.

Figure 2a recorded a wide TSC signal when 10.5 mole% Ge was added, ascribed to the presence of severe trap states distribution (typically the deep traps); with a huge total trap density of 5.26×10^{21} cm^{-3} (Figure 2b).[17,32] We found that the recorded enormous trap densities when 10.5 mole% Ge was added were not attributed to the Sn^{2+} vacancy, but it could be due to the distortion or the destabilized perovskite framework caused by the thickening of GeO_2. As evidenced through XPS profile (Figure S4d), FPSGI (10.5 Ge) exhibited the least Sn^{4+}/Sn^{2+} ratio, but with intense GeO_2 peak (Figure S4e). Although the role of Ge in suppressing the oxidation of Sn^{2+} has been certified, however, the over-thickening GeO_2 has worsen the charge transportation. It is notable that the large increase in current at high temperature region is not owing to the release of trap

carriers, but it could be due to leakage current or thermally activated atomic vacancies.[30,33,34]

As depicted in Figure 2b, it is cleared that trap states and defects (FPSGI (10.5 Ge)) were severely formed at a deeper trap level from -0.6 eV onwards, which significantly impact the V_{oc} (higher energy loss) of the device owing to energy disorder.[35] This phenomenon could be the downside of excessive Ge ions which have worsen the film formation, as observed through the morphological structure of FPSGI (10.5Ge) where pinholes (yellow circles) are observed on the perovskite surface. While, when an optimum amount of Ge (7.5 mole%) was incorporated, the shallow trap density was substantially minified from 10^{15} cm^{-3} (0 mole% Ge) to 10^{13} cm^{-3} due to the passivation effect of Ge ions; as evidences through smaller TSC signal in Figure 2a. The activation energy, E_a of the trap states can be identified through initial rise method from the Arrhenius plot from 94 K-286 K, as depicted in equation (3):[36]

$$I_{TSC} \propto \exp\left(-E_t/kT\right) \quad (3)$$

where I_{TSC} is the TSC in the initial rise regime, k is the Boltzmann constant, and T is the temperature.

The succession in trap states passivation can be further verified through the reduction of energetic trap states of Ge-based device from an E_a of 252 meV (0 mole% Ge) to 215 meV (Figure S5).[32] It is thus ascertained that Ge has an effect to remove detrimental traps or shift traps closer to the valence or conduction band in the perovskite vicinity, but not the PEAI.[32] In great agreement with the TSC

evaluation, the density of states (DOS) distribution of Figure 2c manifested that the Ge-based device has fewer number of available states for electrons to occupy.[17,37] The beneficial role of Ge was further demonstrated by correlating the carrier concentration and trap density of the perovskite films. As observed in Figure 2d, FPSGI (7.5Ge) perovskite exhibited the least trap density and carrier concentration, as compared to the FPSGI (0Ge). Thus, we conclude that the Ge is a perfect ingredient for defects passivation, background carrier densities reduction, and to minify Sn vacancies formation, which is an important additive to suppress recombination and V_{oc} loss.

To rationalize the charge recombination mechanism, we performed impedance spectroscopy measurements under dark at open circuit condition and the Nyquist plots were fitted by the equivalent model, as displays in Figure 3a. It is notable that lower series resistance, R_s enhances charge transportation, while larger charge recombination resistance, R_{rec} indicates lower recombination rate.[38,39] Expectedly, the Ge-based solar cells; excepting FPSGI (10.5Ge) and Ge-free device; exhibited larger R_{rec} (larger semicircle), which in regard to less trap density formation (Figure 3b), indicates remarkable suppression of interfacial charge recombination; credited to defect passivation by the Ge.[40,41] The succession of Ge in trap states passivation and Sn^{2+} vacancy suppression is also verified when FPSGI (7.5Ge) exhibited higher R_{sh} than the devices without Ge additive, implies the device possesses higher resistance to increase carrier density caused by self p-doping. The exceptional case for FPSGI (10.5Ge) could be first owing to the excessive doping of Ge, which is anticipated to have distorted the perovskite framework.

Secondly, the formation of the dense GeO_2 layer (proven through XPS profile in Figure S4e) might have severely hampered charge transportation. To further analyze the charge recombination mechanism and V_{oc} improvement, we then performed the capacitance-voltage (C-V) measurement. Consistently, the larger flat band potential (V_{bi}) of the FPSGI (7.5Ge) device than the Ge-free devices (Figure 3d) implies better charge transport, separation, and collection of carriers.[12] Comparatively, the Ge-free devices exhibited the least V_{bi} (consistent with R_{rec} value), indicative of the happening of severe charge recombination at the trap states, especially at deeper trap level (corroborated to the TSC profile). In addition, the passivation effect of Ge is further verified through transient photovoltage (TPV) and transient photocurrent (TPC). Figure S6a manifests that the decay time of the mixed 2D/3D perovskite with Ge under open-circuit condition (TPV) is longer than the perovskite without Ge, indicative of less non-radiative recombination sites (consistent with the TSC results). Whilst, the TPC profile (Figure S6b) illustrates that the decay time of perovskite with Ge is quicker, implies the Ge-based perovskite exhibited better charge carrier extraction capability than the Ge-free perovskite. This phenomenon could be credited to the enhanced perovskite morphology upon Ge addition (pinhole-less), in addition the alteration of the perovskite's electronic structure by the Ge ion, which consequently shifted the Ge-perovskite valence bands to match the hole-transporting layer (Figure S7).[42] The capability of Ge in traps passivation and Sn^{4+} suppression has significantly improved the carrier dynamics of the FPSGI (7.5Ge); with an achievable high mobility of 70.65 $cm^2V^{-1}s^{-1}$. Relatively, the charge mobility for the FPSGI (0Ge)

perovskite was compromised due to the occurrence of severe recombination process (low R_{rec} = 21.2 kΩ).

Conclusion

In summary, we have highlighted the importance and effectiveness of Ge in traps passivation and thanks to the synergism between PEAI and GeI_2 in stabilizing the mixed 2D/3D perovskite lattice. The Ge plays an important role in suppressing defect/trap states, as deduced through TSC evaluation. The addition of an optimum amount of Ge reduced carrier trapping at the surfaces and grain boundaries, as evidenced that the addition of 7.5 mole% Ge has doubly reduced the trap densities from $9.68x10^{20}$ cm^{-3} (FPSGI (0Ge)) to $4.14x10^{20}$ cm^{-3}, which is in great agreement with the DOS distribution. It was also assured that Ge addition could suppress Sn^{2+} oxidation process, as proven through the XPS, which is an important finding for high photovoltaic performances. The effectiveness of Ge in passivating traps and suppressing Sn^{2+} vacancy was also explicated through the reduction of carrier densities upon the addition of Ge, which led to high mobility of 70.65 $cm^2V^{-1}s^{-1}$. Effectively, the FPSGI (7.5Ge) solar cell recorded a high efficiency of 7.45%, high J_{sc} of 21.92 mA/cm^2, and high V_{oc} of 0.46 V with excellent stability at ambient condition.

Experimental

Perovskite Solar Cell Fabrication: The FTO glass was first cleaned through ultrasonic bath using lab detergent (SCAT 20-X, Japan), distilled water, acetone, isopropanol, and distilled water for 10min, respectively. Subsequently, the glasses were dried and subjected for plasma treatment (electronic Diener, Plasma-surface-

technology, Germany) for 5 min prior to the spin coating process. The PEDOT:PSS used as a hole transport material was spin coated at 5000 rpm for 50 s, followed by heating treatment at 140 ºC for 20 min to completely evaporate the water. The coated samples were then transferred and kept inside the N_2 gas circulated glovebox, and the subsequent coating processes were done inside the glovebox. 0.92 M FAI, 0.08 M PEAI, (1-x M) SnI_2, x M GeI_2, and 0.1 M SnF_2 were stirred in DMF:DMSO in a 4:1 ratio. 50 µl of the perovskite precursor solution was spin coated on the PEDOT:PSS coated substrate at 5000 for 50 s. 500 µl chlorobenzene was casted at 13-15 s and the film was completed by annealing at 70 ºC for 10 min. Next, 25 nm C60, 6 nm BCP, 70 nm Ag, and 30 nm Au were sequentially deposited by thermal evaporation process.

Conflict of Interest

The authors declare no conflict of interest.

Acknowledgements

This research was supported by JST MiraiProgram.

References

1 W. Gao, C. Ran, J. Li, H. Dong, B. Jiao, L. Zhang, X. Lan, X. Hou and Z. Wu, *Journal of Physical Chemistry Letters*, 2018, **9**, 6999–7006.

2 Y. Dang, Y. Zhou, X. Liu, D. Ju, S. Xia, H. Xia and X. Tao, *Angewandte Chemie - International Edition*, 2016, **55**, 3447–3450.

3 S. Shao, J. Liu, G. Portale, H. H. Fang, G. R. Blake, G. H. ten Brink, L. J. A. Koster and M. A. Loi, *Advanced Energy Materials*, 2018, **8**, 1702019.

4 S. Shao, J. Dong, H. Duim, G. H. ten Brink, G. R. Blake, G. Portale and M. A. Loi, *Nano Energy*, 2019, **60**, 810–816.

5 M. Konstantakou and T. Stergiopoulos, *Journal of Materials Chemistry A*, 2017, **5**, 11518–11549.

6 W. Liao, D. Zhao, Y. Yu, C. R. Grice, C. Wang, A. J. Cimaroli, P. Schulz, W. Meng, K. Zhu, R. G. Xiong and Y. Yan, *Advanced Materials*, 2016, **28**, 9333–9340.

7 H. Kim, Y. H. Lee, T. Lyu, J. H. Yoo, T. Park and J. H. Oh, *Journal of Materials Chemistry A*, 2018, **6**, 18173–18182.

8 T. Bin Song, T. Yokoyama, S. Aramaki and M. G. Kanatzidis, *ACS Energy Letters*, 2017, **2**, 897–903.

9 N. K. Noel, S. D. Stranks, A. Abate, C. Wehrenfennig, S. Guarnera, A. A. Haghighirad, A. Sadhanala, G. E. Eperon, S. K. Pathak, M. B. Johnston, A. Petrozza, L. M. Herz and H. J. Snaith, *Energy and Environmental Science*, 2014, **7**, 3061–3068.

10 T. Leijtens, R. Prasanna, A. Gold-Parker, M. F. Toney and M. D. McGehee, *ACS Energy Letters*, 2017, **2**, 2159–2165.

11 C. H. Ng, H. N. Lim, S. Hayase, Z. Zainal and N. M. Huang, *Renewable and Sustainable Energy Reviews*, 2018, **90**, 248-274.

12 E. Jokar, C. H. Chien, A. Fathi, M. Rameez, Y. H. Chang and E. W. G. Diau, *Energy and Environmental Science*, 2018, **11**, 2353–2362.

13 A. Al Mamun, T. T. Ava, H. J. Jeong, M. S. Jeong and G. Namkoong, *Physical Chemistry Chemical Physics*, 2017, **19**, 9143–9148.

14 D. W. DeQuilettes, S. M. Vorpahl, S. D. Stranks, H. Nagaoka, G. E. Eperon, M. E. Ziffer, H. J. Snaith and D. S. Ginger, *Science*, 2015, **348**, 683–686.

15 M. H. Kumar, S. Dharani, W. L. Leong, P. P. Boix, R. R. Prabhakar, T. Baikie, C. Shi, H. Ding, R. Ramesh, M. Asta, M. Graetzel, S. G. Mhaisalkar and N. Mathews, *Advanced Materials*, 2014, **26**, 7122–7127.

16 S. J. Lee, S. S. Shin, Y. C. Kim, D. Kim, T. K. Ahn, J. H. Noh, J. Seo and S. Il Seok, *Journal of the American Chemical Society*, 2016, **138**, 3974–3977.

17 C. H. Ng, K. Nishimura, N. Ito, K. Hamada, D. Hirotani, Z. Wang, F. Yang, S. Likubo, Q. Shen, K. Yoshino, T. Minemoto and S. Hayase, *Nano Energy*, 2019, **58**, 130–137.

18 N. Ito, M. A. Kamarudin, D. Hirotani, Y. Zhang, Q. Shen, Y. Ogomi, S. Iikubo, T. Minemoto, K. Yoshino and S. Hayase, *Journal of Physical Chemistry Letters*, 2018, **9**, 1682–1688.

19 L. N. Quan, M. Yuan, R. Comin, O. Voznyy, E. M. Beauregard, S. Hoogland, A. Buin, A. R. Kirmani, K. Zhao, A. Amassian, D. H. Kim and E. H. Sargent, *Journal of the American Chemical Society*, 2016, **138**, 2649–2655.

20 H. Tsai, W. Nie, J. C. Blancon, C. C. Stoumpos, R. Asadpour, B. Harutyunyan, A. J. Neukirch, R. Verduzco, J. J. Crochet, S. Tretiak, L. Pedesseau, J. Even, M. A. Alam, G. Gupta, J. Lou, P. M. Ajayan, M. J. Bedzyk, M. G. Kanatzidis and A. D. Mohite, *Nature*, 2016, **536**, 312–317.

21 Y. Hu, J. Schlipf, M. Wussler, M. L. Petrus, W. Jaegermann, T. Bein, P. Müller-Buschbaum and P. Docampo, *ACS Nano*, 2016, **10**, 5999–6007.

22 C. Ma, C. Leng, Y. Ji, X. Wei, K. Sun, L. Tang, J. Yang, W. Luo, C. Li, Y. Deng, S. Feng, J. Shen, S. Lu, C. Du and H. Shi, *Nanoscale*, 2016, **8**, 18309–18314.

23 D. H. Cao, C. C. Stoumpos, T. Yokoyama, J. L. Logsdon, T. Bin Song, O. K. Farha, M. R. Wasielewski, J. T. Hupp and M. G. Kanatzidis, *ACS Energy Letters*, 2017, **2**, 982–990.

24 Y. Liao, H. Liu, W. Zhou, D. Yang, Y. Shang, Z. Shi, B. Li, X. Jiang, L. Zhang, L. N. Quan, R. Quintero-Bermudez, B. R. Sutherland, Q. Mi, E. H. Sargent and Z. Ning, *Journal of the American Chemical Society*, 2017, **139**, 6693–6699.

25 W. Ke, C. C. Stoumpos, M. Zhu, L. Mao, I. Spanopoulos, J. Liu, O. Y. Kontsevoi, M. Chen, D. Sarma, Y. Zhang, M. R. Wasielewski and M. G. Kanatzidis, *Science Advances*, 2017, **3**, 1701293.

26 C. H. Ng, T. S. Ripolles, K. Hamada, S. H. Teo, H. N. Lim, J. Bisquert and S. Hayase, *Scientific Reports*, , 2018, **8**, 2482.

27 W. Ke, C. C. Stoumpos, I. Spanopoulos, M. Chen, M. R. Wasielewski and M. G. Kanatzidis, *ACS Energy Letters*, 2018, **3**, 1470–1476.

28 Q. Zhu, X. Bao, J. Yu, D. Zhu, M. Qiu, R. Yang and L. Dong, *ACS Applied Materials and Interfaces*, 2016, **8**, 2652–2657.

29 B. Cai, Y. Xing, Z. Yang, W. H. Zhang and J. Qiu, *Energy and Environmental*

Science, 2013, **6**, 1480–1485.

30 C. Qin, T. Matsushima, T. Fujihara, W. J. Potscavage and C. Adachi, *Advanced Materials*, 2016, **28**, 466–471.

31 G. Kapil, T. Bessho, C. H. Ng, K. Hamada, M. Pandey, M. A. Kamarudin, D. Hirotani, T. Kinoshita, T. Minemoto, Q. Shen, T. Toyoda, T. N. Murakami, H. Segawa and S. Hayase, *ACS Energy Letters*, 2019, **4**, 1991-1998.

32 Y. Hu, E. M. Hutter, P. Rieder, I. Grill, J. Hanisch, M. F. Aygüler, A. G. Hufnagel, M. Handloser, T. Bein, A. Hartschuh, K. Tvingstedt, V. Dyakonov, A. Baumann, T. J. Savenije, M. L. Petrus and P. Docampo, *Advanced Energy Materials*, 2018, **8**, 1–11.

33 S. D. Stranks, V. M. Burlakov, T. Leijtens, J. M. Ball, A. Goriely and H. J. Snaith, *Physical Review Applied*, 2014, **2**, 034007.

34 I. A. Shkrob and T. W. Marin, *Journal of Physical Chemistry Letters*, 2014, **5**, 1066–1071.

35 I. Lange, J. Kniepert, P. Pingel, I. Dumsch, S. Allard, S. Janietz, U. Scherf and D. Neher, *Journal of Physical Chemistry Letters*, 2013, **4**, 3865–3871.

36 J. Schafferhans, A. Baumann, C. Deibel and V. Dyakonov, *Applied Physics Letters*, 2008, **93**, 093303.

37 S. Teo, Z. Guo, Z. Xu, C. Zhang, Y. Kamata, S. Hayase and T. Ma, *ChemSusChem*, 2019, **12**, 518-526.

38 F. Yang, M. A. Kamarudin, G. Kapil, D. Hirotani, P. Zhang, C. H. Ng, T. Ma and S. Hayase, *ACS Applied Materials and Interfaces*, 2018, **10**, 24543–24548.

39 P. Zhang, F. Yang, G. Kapil, C. H. Ng, T. Ma and S. Hayase, *ACS Sustainable Chemistry and Engineering*, 2019, **7**, 3956-3961.

40 Z. Wang, A. K. Baranwal, M. A. kamarudin, C. H. Ng, M. Pandey, T. Ma and S. Hayase, *Nano Energy*, 2019, **59**, 258-267.

41 Z. Wang, M. A. Kamarudin, N. C. Huey, F. Yang, M. Pandey, G. Kapil, T. Ma and S. Hayase, *ChemSusChem*, 2018, **11**, 3941-3948.

42 Z. Wang, A. Pradhan, M. A. Kamarudin, M. Pandey, S. S. Pandey, P. Zhang, C. H. Ng, A. S. M. Tripathi, T. Ma and S. Hayase, *ACS Applied Materials and Interfaces*, 2019, **11**, 10012-10020.

Figures

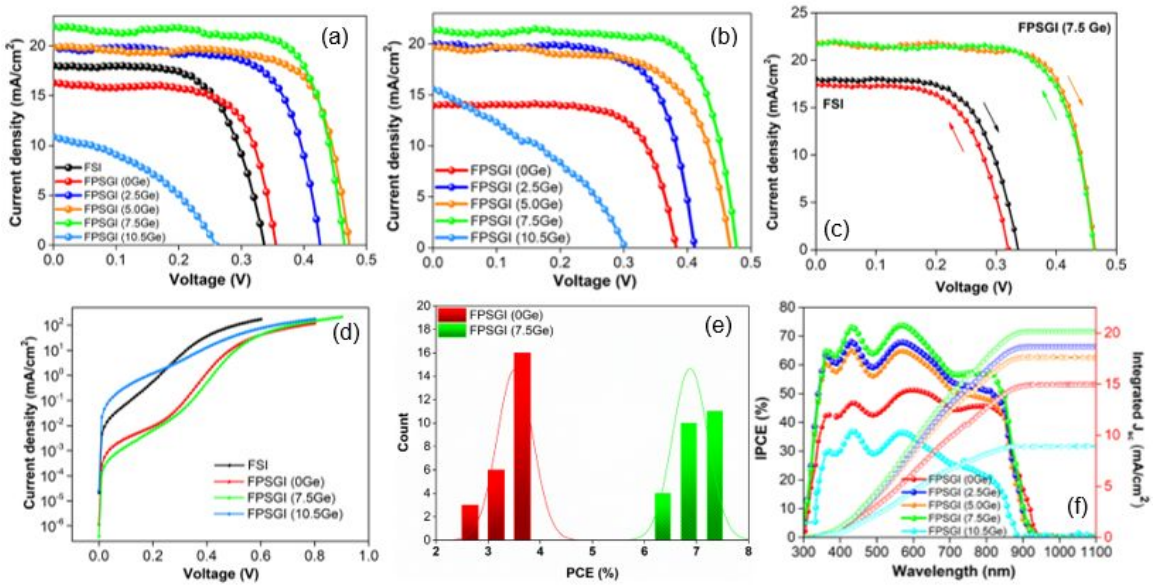

Figure 1. J-V profiles of (a) fresh and (b) after 192h 2DGe perovskite solar cells at various Ge concentrations. (c) hysteresis, (d) dark current density, (e) histogram composed of 25 devices, and (f) IPCE and integrated J_{sc} of $FPS_xG_{1-x}I_3$ perovskite solar cells. The stability measurement was performed in a glovebox.

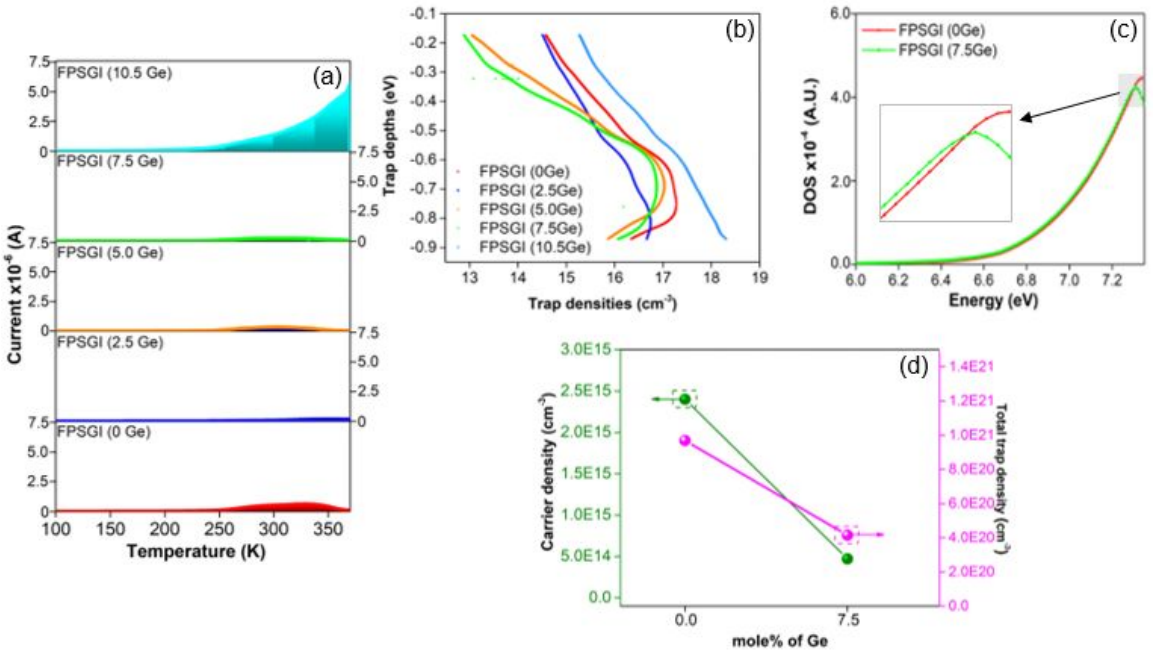

Figure 2. (a) Current-temperature profile, (b) TSC profile, (c) density of states distribution (DOS), and (d) relationship between carrier concentration and total trap density of the $FPS_xG_{1-x}I_3$ perovskite films. The carriers concentration of the perovskite materials were measured via hall measurement.

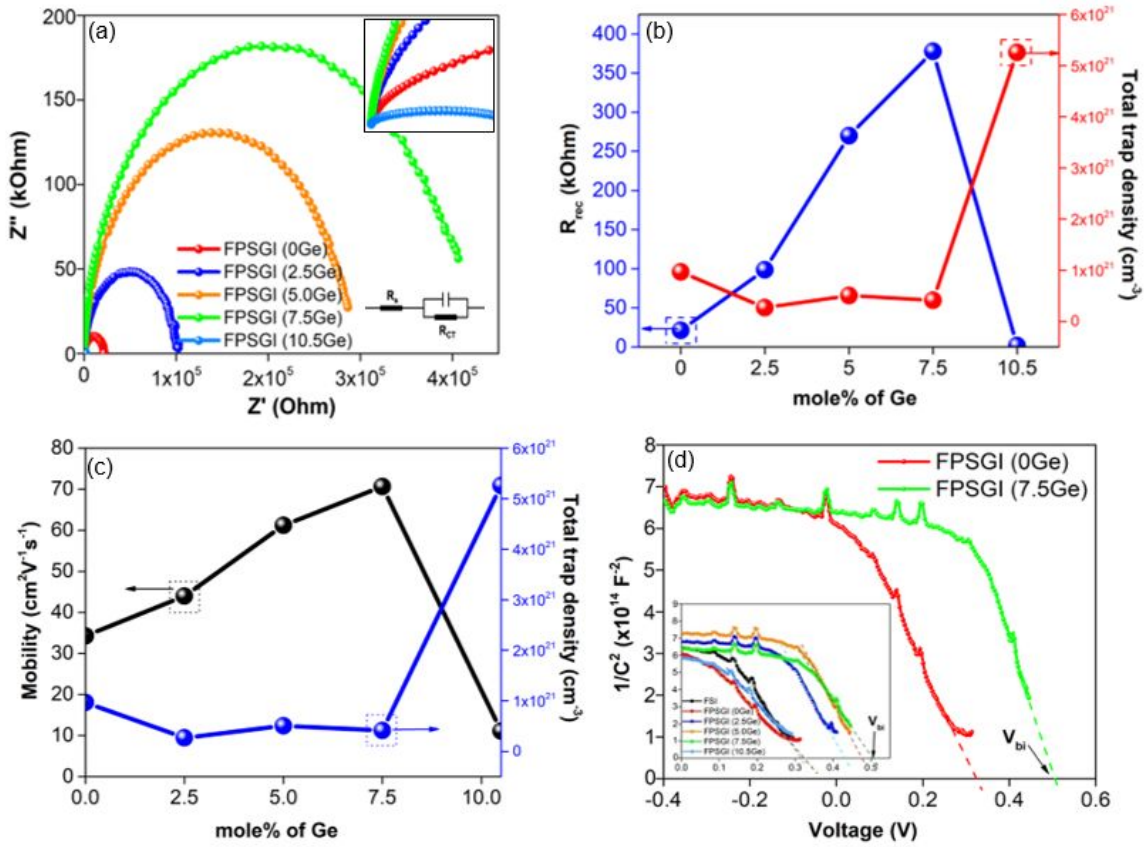

Figure 3. (a) Nyquist plots, (b) relationship between recombination resistance (R_{rec}) and total trap density, (c) mobility versus total trap density, and (d) capacitance-voltage of $FPS_xG_{1-x}I_3$ perovskite solar cells.

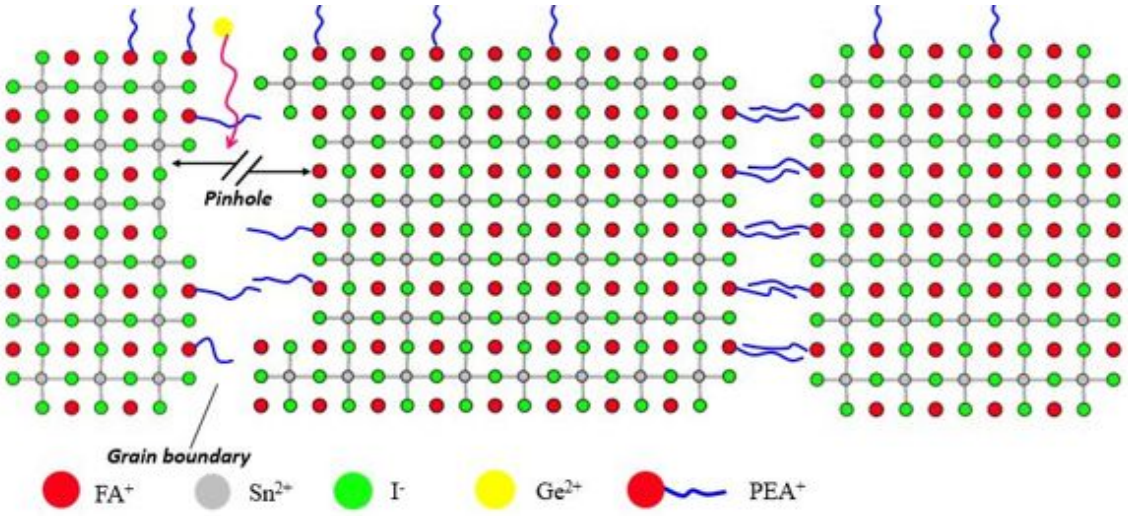

Scheme 1. shows the passivation effect of Ge within the perovskite lattice.

Tables

Table 1. Photovoltaic performances of $FPS_{1-x}G_xI_3$ perovskite solar cells at different Ge concentrations.

Perovskites	J_{sc} (mA/cm^2)	V_{oc} (V)	FF	PCE (%)
$FASnI_3$ (FSI)	17.99	0.34	0.64	3.86
FPSGI (0Ge)	16.27	0.36	0.68	3.92
FPSGI (2.5Ge)	19.85	0.43	0.69	5.84
FPSGI (5.0Ge)	19.84	0.47	0.72	6.80
FPSGI (7.5Ge)	21.92	0.46	0.73	7.45
FPSGI (10.5Ge)	10.85	0.26	0.40	1.14

Table 2. Carrier kinetics of $FPS_xG_{1-x}I_3$ perovskite films with and without Ge.

Perovskites	Total trap densities (cm^{-3})	Carrier density (cm^{-3})	Sn^{4+}/Sn^{2+} Ratio	Activation energy, E_a (meV)
Without Ge	9.68×10^{20}	2.39×10^{15}	1.24	252
With Ge	4.14×10^{20}	4.73×10^{14}	0.71	214

Table 3. Tabulated series resistance (R_s), recombination resistance (R_{rec}), and mobility of the $FPS_{1-x}G_xI_3$ devices. The R_s and R_{rec} were obtained from impedance spectroscopy.

Perovskites	R_s (Ω)	R_{rec} (kΩ)	Mobility, μ ($cm^2V^{-1}s^{-1}$)
FSI	4.56	7.78	23.39
FPSGI (0Ge)	3.40	21.2	34.28
FPSGI (2.5Ge)	3.23	98.6	43.97
FPSGI (5.0Ge)	3.96	270	61.19
FPSGI (7.5Ge)	4.62	378	70.65
FPSGI (10.5Ge)	3.41	1.91	11.10

The incorporation of GeI_2 additive on a new type quasi-2D/3D Sn perovskite **suppresses Sn^{2+} oxidation and trap densities, thus merits the carrier dynamics** of the perovskite materials.